Influence of interatomic bonding potentials on detonation properties

Andrew J. Heim and Niels Grønbech-Jensen
Department of Applied Science, University of California, Davis, California 95616, USA and Computational Research Division, Lawrence Berkeley National Laboratory, Berkeley, California 94720, USA

Timothy C. Germann and Brad Lee Holian
Applied Physics Division, Los Alamos National Laboratory, Los Alamos, New Mexico 87545, USA

Edward M. Kober* and Peter S. Lomdahl
Theoretical Division, Los Alamos National Laboratory, Los Alamos, New Mexico, 87545, USA
(Received 23 December 2005; revised manuscript received 16 December 2006; published 29 August 2007)

The dependences of the macroscopic detonation properties of a two-dimensional (2D) diatomic (AB) molecular system on the fundamental molecular properties were investigated. This includes examining the detonation velocity, reaction zone thickness, and critical width as functions of the exothermicity (Q) of the gas-phase reaction [$AB \rightarrow (1/2)(A_2+B_2)$] and the gas-phase dissociation energy (D_e^{AB}) for $AB \rightarrow A+B$. Following previous work, molecular dynamics (MD) simulations with a reactive empirical bond-order potential were used to characterize the shock-induced response of a diatomic AB molecular solid, which exothermically reacts to produce A_2 and B_2 gaseous products. Nonequilibrium MD simulations reveal that there is a linear dependence between the square of the detonation velocity and both of these molecular parameters. The detonation velocities were shown to be consistent with the Chapman–Jouguet (CJ) model, demonstrating that these dependences arise from how the equation of state of the products and reactants are affected. Equilibrium MD simulations of microcanonical ensembles were used to determine the CJ states for varying Q's, and radial distribution functions characterize the atomic structure. The character of this material near the CJ conditions was found to be somewhat unusual, consisting of polyatomic clusters rather than discrete molecular species. It was also found that there was a minimum value of Q and a maximum value of D_e^{AB} for which a pseudo-one-dimensional detonation could not be sustained. The reaction zone of this material was characterized under both equilibrium (CJ) and transient (underdriven) conditions. The basic structure is consistent with the Zeldovich–von Neumann-Döring model, with a sharp shock rise and a reaction zone that extends to 200–300 Å. The underdriven systems show a buildup process which requires an extensive time to approach equilibrium conditions. The rate stick failure diameter (critical width in 2D) was also found to depend on Q and D_e^{AB}. The dependence on Q could be explained in terms of the reaction zone properties.

DOI: 10.1103/PhysRevE.76.026318 PACS number(s): 47.40.Rs, 47.50.Cd, 82.40.Fp, 47.11.Mn

I. INTRODUCTION

The simplest theory of detonation is that of Chapman and Jouguet (CJ) [1–3]. In this one-dimensional theory the shock rise and reaction are treated as instantaneous. On a pressure-specific volume (P-v) state diagram the point of tangency between a Rayleigh line (an expression of the conservations of mass and momentum across the detonation front traveling at a given velocity) and a Hugoniot (conservation of energy) is the CJ state. The slope of the Rayleigh line is proportional to the negative of the square of the product of the initial density (ρ_0) of the material and the detonation velocity (u_s). If u_s is any slower than the CJ value (u_{sj}), the Rayleigh line does not intersect the Hugoniot, and there is no solution to the conservation equations. In this light the CJ state is determined by the equation of state (EOS) of the products and the initial state of the reactants, and that determines the minimum sustainable detonation velocity ($=u_{sj}$) for the system. This hypothesis predicts the detonation properties of high-performance explosives reasonably well despite its crude assumption [1,2].

A more detailed model is the classical theory of detonation due to Zeldovich [4], von Neumann [5], and Döring [6] (ZND) which, following the initial shock compression, allows the molecules of a high explosive (HE) to react and expand. This is represented by a pressure profile, whose principal features are (i) an instantaneous shock rise to a state where the reactants are heated and compressed, typically referred to as the von Neumann spike (vNS); (ii) a fixed-width reaction zone, in which an irreversible reaction provides the chemical energy to maintain the detonation wave as density and pressure decrease; and (iii) a Taylor wave of the rarefying (expanding) product gases. In the case where the detonation is supported by a driving piston, there will be a constant state in the pressure profile from some point behind the reaction zone back to the piston. If the piston is driven at the particle velocity of the unsupported final state (matching the CJ state at the end of the reaction zone), there will be no Taylor wave and only the reaction zone will be observed. If the piston is driven at a greater velocity than this critical value, the detonation velocity will be increased. The detonation is now said to be overdriven, and the flow in the constant zone is subsonic in the frame of the detonation front. For the case where the detonation is underdriven with respect to the CJ conditions, it should asymptotically approach the

*emk@lanl.gov

minimum detonation velocity determined by the CJ state, and only the Taylor expansion will be affected by a disturbance behind the final state [1].

When more complex reaction schemes are considered, the situation could become significantly more complicated. Steady solutions are still feasible, but propagation characteristics could be determined by the properties of an incompletely reacted state. Such solutions could also correspond to either the weak or strong detonation branches [1]. Unsteady solutions are also possible, as have been studied by several authors [7–10]. Here, the propagation characteristics are highly dependent upon the reaction scheme and the EOS along that reaction path. Such instabilities are regularly observed for gas-phase detonations. For condensed-phase explosives, there are open questions as to what the fine-scale structure of the detonation wave is, how accurate one can expect the CJ model to be, and how this is controlled by the material properties and reaction characteristics [10]. Generally, there is good agreement ($\approx 5\%$) between the predictions of CJ theory and current molecular models for the product equations of state [2,11–14], but this is not sufficient to resolve these issues and some of the assumptions of the analysis.

Molecular dynamics (MD) simulations are well suited to test these and other aspects of condensed-phase detonation theory and the associated models under controlled microscopic conditions, as demonstrated by work going back over a decade [15–28]. With MD it is possible to control the inherent material properties, reaction pathways, initial material state, and confinement conditions of the simulation. For example, using a predissociative Morse potential, Maffre and Peyrard performed a preliminary study of "hot spots," which arise at heterogeneities [21]. Later work using more chemically realistic potentials was also done by other groups using voids and gaps as the heterogeneities [26–29]. Monte Carlo techniques have been incorporated with MD to find thermodynamic properties and the Hugoniot of a system of hard spheres [22] and, more recently, a reactive model close to the one used here [18]. Tests of the dependence of the critical flyer plate velocity needed to initiate detonation on the flyer plate thickness [24,30] have been studied. Rice *et al.* have characterized some aspects of the reaction mechanism [19] and demonstrated a correspondence to hydrodynamic theory for a model system [18] as have White *et al.* [30]. With simple adjustments of the MD potentials, it is not normally possible to control the different macroscopic features independently, so it is not always straightforward to perform direct mappings onto the continuum theories. Still, it is a general goal to connect the microscales and macroscales with MD and hydrodynamic codes [28].

Many of these simulations [16–20,23–28] have been conducted in two dimensions using a reactive empirical bond order (REBO) potential [16], representing a simple material composed of two atom types (A and B). REBO is a modification of Tersoff's empirical bond order (EBO) potential [31]. The restriction to two dimensions allows significantly greater spatial and time scales to be accessed for given computational resources, though three-dimensional simulations have also been pursued [20,28]. The process of chemically sustained shock waves, converting reactant AB molecules exothermically into A_2 and B_2 products, is represented in the REBO model of Brenner *et al.* [16]. With this, it has been demonstrated that nonequilibrium MD (NEMD) simulations using REBO potentials produce detonations consistent with both continuum theory and experimental observations [20]. However, it has been found that seemingly subtle variations in the model or parameters can result in rather dramatic changes in behavior [20,32]. Also, because of intense computational requirements, many simulations have been limited in scale such that significant features are not always resolved.

Our goal in this work is to thoroughly document the behavior of one of these models and gain a better understanding of the physical basis of its response characteristics. By utilizing large-scale simulations done with the SPASM parallel MD code [33], we are able to extend the spatial and dynamic range of the simulations and provide stronger bounds on the results. Our aim is to extend the innovative work of Haskins *et al.* [25] and Elert *et al.* [34,35] by investigating the dependences of the detonation velocity, the reaction zone thickness, and the critical width that a HE must have in transverse directions to sustain detonation in these atomistic simulations. This will be done with controlled variations in the fundamental microscopic energetic quantities—namely, the exothermicity (Q) of the reaction and AB dissociation energy (D_e^{AB})—in order to document more thoroughly the relationship between microscopic properties and macroscopic behavior. Complementing this, we also characterize the EOS of the products, particularly around the CJ state, and show how this relates to the reaction pathway. This establishes a benchmark with which other methods can be compared in order to establish the physical basis for different phenomena.

This paper is organized as follows. In Sec. II we lay out the details of the potential used and the simulations performed. In Sec. III, using equilibrium microcanonical (*NVE*) ensembles, we map out the product Hugoniot for set values of the parameters and compare the expected CJ velocities of the detonation fronts to those found by unsupported NEMD simulations. The CJ states of these materials are also characterized here. In Sec. IV we study the relationship of Q to the EOS in order to better understand the results from Sec. III. In Sec. V we characterize the width of the reaction zone and compare this to the critical minimum width (W_c) which a two-dimensional (2D) sample must have in the direction normal to the propagating detonation front in order for that detonation to be sustained. (In 3D cylindrical samples, of course, the critical width analog is known as the failure diameter, and the experimental setup is called a rate stick.)

II. METHODS

There are several versions of REBO used in the related literature. The version used here is due to Brenner *et al.* [16] and is called Model I in Ref. [30]. In it the binding energy of an N-atom system takes the form

$$E_b = \sum_{i}^{N} \sum_{j>i}^{N} \{f_c(r_{ij})[V_R(r_{ij}) - \bar{B}_{ij} V_A(r_{ij})] + V_{\mathrm{vdW}}(r_{ij})\}, \quad (1)$$

where r_{ij} is the distance from atom i to atom j. V_A and V_R are the attractive and repulsive terms, respectively, of a Morse

intramolecular potential $V_A - V_R$, and $\bar{B}_{ij} \equiv (B_{ij}+B_{ji})/2$, which contains the effective valence interactions and is designed to favor dimer formation. Depending on the local environment, $\bar{B}_{ij}$ varies from 0 to 1. If atom i has no neighbors [defined by the smooth cutoff function $f_c(r)$] other than j, then $B_{ij}=1$ and the full Morse attraction is felt. On the other hand, if i has two neighbors j and k, and $r_{ij}<r_{ik}$, then $0<B_{ik}<B_{ij}<1$; i.e., the ij and ik attractions are both reduced, but more so for the pair farther apart (ik) than for the nearer pair (ij). The effect of this is to introduce a preferential valence of one for each atom. A weak intermolecular van der Waals (Lennard-Jones form) interaction V_{vdW} stabilizes a crystalline AB molecular solid, at least at low temperatures. The rest of the precise functional forms and parameters are contained in the errata of [16].

Isolated XY molecules ($X, Y \in \{\mathrm{A}, \mathrm{B}\}$) have binding energies D_e^{XY} (since $\bar{B}_{ij}=1$). These are the fundamental parameters that we will vary from their base-line values [16], $D_e^{\mathrm{AA}}=D_e^{\mathrm{BB}}=5.0$ eV and $D_e^{\mathrm{AB}}=2.0$ eV. These two parameters (constraining $D_e^{\mathrm{AA}}=D_e^{\mathrm{BB}}$) are related to the exothermicity (Q) through

$$2\mathrm{AB} \rightarrow \mathrm{A}_2 + \mathrm{B}_2 + 2Q, \tag{2a}$$

$$Q = D_e^{\mathrm{AA}} - D_e^{\mathrm{AB}}. \tag{2b}$$

D_e^{AB} is just the energy required to dissociate an isolated AB molecule:

$$\mathrm{AB} + D_e^{\mathrm{AB}} \rightarrow \mathrm{A} + \mathrm{B}. \tag{3}$$

Q is varied from 1.5 eV to 10.0 eV by holding D_e^{AB} constant at 2.0 eV while D_e^{AA} is varied from 3.5 eV to 12.0 eV. D_e^{AB} is varied from 0.5 to 3.5 eV by varying D_e^{AB} and D_e^{AA} together so that their difference Q is constant at 3.0 eV.

In each NEMD setup a stable A_2 flyer plate, four cells thick (two A_2 dimers per cell), impacts a 2D metastable AB herringbone lattice at $z=0$ with a velocity of 9.8227 km/s (Fig. 1). The sample has an initial temperature of 11.6 K. (The potential parameters roughly correspond to N_2, with a correspondingly low melting and boiling point.) The resulting unsupported shock travels to the right, $\hat{z}>0$. In $\hat{z}$ the boundaries are culled; i.e., particles are lost when they exit the simulation cell. In the lateral $\hat{x}$ direction the boundaries are periodic in Sec. III to study planar detonations, or culled, but padded with free space, in Sec. V to determine failure widths. In computations involving the reaction zone thickness and detonation velocity, the sample initially is at least 48 lattice cells in $\hat{x}$ and 600 in $\hat{z}$. The simulation is allowed to run for at least 30.54 ps with a time step $dt=0.25$ fs. The minimum duration is the same for trials determining W_c versus either Q or D_e^{AB}. The maximum length for these calculations is 360 cells in $\hat{z}$. In the equilibrium MD calculations presented in Sec. IV, the samples are 25×25 cells^2 with periodic boundary conditions. These simulations are run for 40 ps with measurements averaged over the last 30 ps.

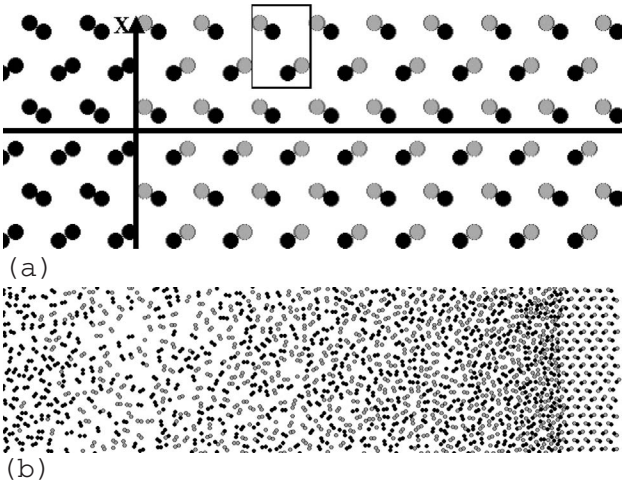

FIG. 1. (a) A snapshot of a magnified section of the initial sample in a flyer driven unsupported NEMD simulation of detonation at $t=0$. The A atoms are black and the B gray. The A_2 flyer plate can be seen to the left of the x axis. The box encloses a herringbone lattice cell, consisting of two AB dimers. (b) A snapshot of the detonating sample with the detonation front moving toward the right.

III. DETONATION VELOCITY AND THE CJ CONDITIONS

Haskins *et al.* and Elert *et al.* have previously reported a linear dependence of u_s^2 on Q for a similar AB material [25,34]. We repeat these studies and further them by varying the AB dissociation energy (D_e^{AB}). One expects the velocity to increase with Q because the increased exothermicity of the reaction increases the temperature and pressure of the products. Figure 2 confirms the linear relationship between u_s^2 and Q for this particular system over a substantial range. The differences between values in Fig. 2 and [25] are due to differences in other REBO parameters and the flyer's thickness and impact velocity. At values of $Q<1.5$ eV, the linear relationship begins to fail, and the system would not sustain a propagating detonation for $Q=1.3$ eV for the initiation impact parameters used here. One of the earlier studies [24] had a lower cutoff value but used slightly different parameters. This failure point likely arises because the reaction rate (determined by the temperature at the initial shock front) has become sufficiently slow such that it does not approach completion within the subsonic region of the reaction zone [1]. The temperature at the shock front can be estimated from the kinetic energy of the shock front, given by the right-hand axis labels in Fig. 2.

The dependence of u_s^2 on D_e^{AB} is also found to be linear and increasing (Fig. 2). Our initial expectation was that the variations in D_e^{AB} would primarily affect the activation energy of the reaction and could quench the detonation when the activation energy became too great to be readily overcome at the temperature of the initial shock state. The failure to maintain a propagating detonation for $D_e^{\mathrm{AB}}>3.7$ eV is possibly a manifestation of this. The strong dependence of u_s^2 on D_e^{AB} indicates that other aspects of the system are likely being affected by this perturbation.

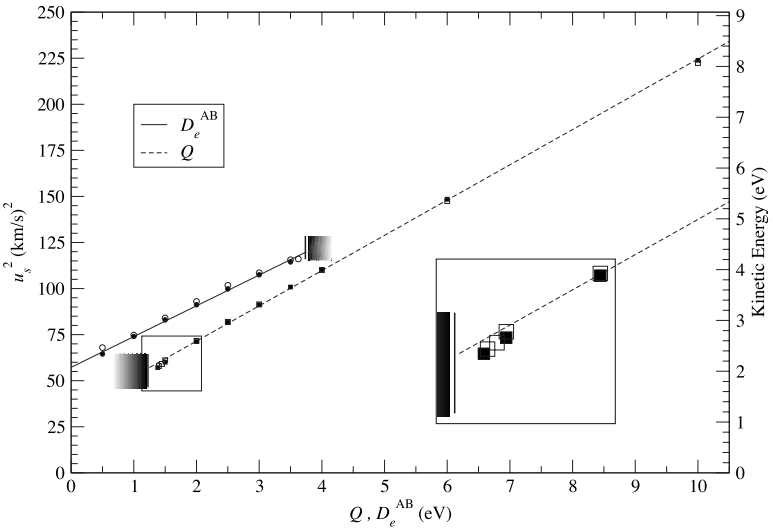

FIG. 2. Square of the detonation velocity (u_s^2) vs AB dissociation energy (D_e^{AB}) and exothermicity (Q). The flyer thickness and impact velocity are held fixed, so detonation is not sustained in regions where it is reported to in [25]. Failure is indicated by the shaded boxes. A sustained detonation is defined as not failing within the 600 unit cell length of the sample. Error bars are smaller than the size of the symbols. The scale on the right gives the kinetic energy of an atom traveling at u_s. The solid symbols are from NEMD simulations with a free boundary at $z=0$. The open symbols are from NEMD simulations with a momentum mirror at $z=0$. The linear fits through the free-boundary data are $u_s^2=33.205+19.137Q$ and $u_s^2=57.251+16.694D_e^{AB}$. The inset box is a 3× magnification of the failure region.

To understand these relationships more thoroughly, we turn first to the basic test of standard detonation theory, which is to compare predictions based on the CJ state determined from equilibrium MD simulations with the evaluation of detonation propagation from NEMD studies. Within a propagating but underdriven detonation, there exists a sonic point, at which the sum of the local sound speed and the particle velocity matches the shock velocity at the front. If the reaction has progressed to completion by the arrival of this point, the effective end of the reaction zone, the propagation conditions should match the CJ conditions [1]. If this is an improper assumption and the reaction is incomplete at the arrival time of the sonic point, it would account for a discrepancy between the theoretical and actual detonation velocities, with the observed velocity being lower than predicted. Because chemical reaction rates are usually well described in terms of exponential decays, it would formally be impossible for a reaction to be totally complete at any finite point in time, so some level of discrepancy is to be expected. We also emphasize that the CJ and simple ZND models both assume an irreversible reaction process, which is not consistent with either standard chemical theory or the formulation of the REBO model. It might be asserted that such discrepancies should be negligible, but detailed quantitative evaluations have not been performed for the version of the AB REBO model studied in this paper. However, using another version of the AB model Swanson *et al.* have reported a detonation velocity obtained from their simulations that was only 0.3% lower than that found from their calculated CJ state [32]. On the other hand, for a slightly different REBO model, Rice *et al.* found a detonation velocity from an unsupported simulation that was 6.1% lower than that found from the calculation of their CJ state [18]. The results of Rice *et al.* may be an example of this inconsistency or may arise because a truly steady-state condition was not achieved, although they attribute it to an asymmetry in the particles' masses.

Our procedure for locating the CJ state is described here and is similar to that of Rice *et al.* and Erpenbeck [18,22]. At different values of the specific volume (v), sets of microcanonical (*NVE*) MD simulations of 2500 particles are run for 40 ps, providing sufficient time to equilibrate. The onset of equilibrium is determined by the shape of the time evolution of the average properties of simulation. After each of these reaches a plateau, as determined by visual inspection, the simulation is allowed to continue. A runs test (the length and number of steady increases or decreases in the data's value are compared to a binomial distribution) is performed to determine that the curves are flat with only random fluctuations. At each value of v, the value of specific internal energy (E) is sought that is a solution of the Hugoniot jump condition,

$$\frac{1}{2}(v_0 - v)P = E - E_0 \tag{4}$$

(energy conservation in which $P_0=0$), where $P=\frac{1}{2}(P_{zz}+P_{xx})$ is the hydrostatic pressure, $P_{\alpha\beta}$ is the negative of the corresponding component of the stress tensor and has ideal and virial components, and the subscript 0 indicates the state in front of the detonation front. Once $\langle E\rangle$ is determined for the present value of v, *NVE* ensemble averages $\langle x\rangle$ of other thermodynamic quantities are computed by linear interpolation.

By repeating this procedure for several values of v, the product P-v Hugoniot is determined (Fig. 3). Using the remaining jump conditions, mass conservation

$$u_p/u_s = (v_0 - v)/v_0, \tag{5}$$

and momentum conservation in which $P_0=0$,

$$u_s u_p = v_0 P, \tag{6}$$

one can find u_s as a function of the particle velocity at the final state (u_p). The minimum possible value of u_s is the CJ value [1], so the minimum of u_s versus any thermodynamic parameter is at the CJ value of that parameter (e.g., see Fig. 4). We use the minimum determined by these means as iterative approximations of the CJ state (see Table I under the "CJ Interpolation" column). We refine the process by fitting a quadratic through the points surrounding the minimum. We must be careful to include a domain small enough that a quadratic is a good approximation to the data, yet large

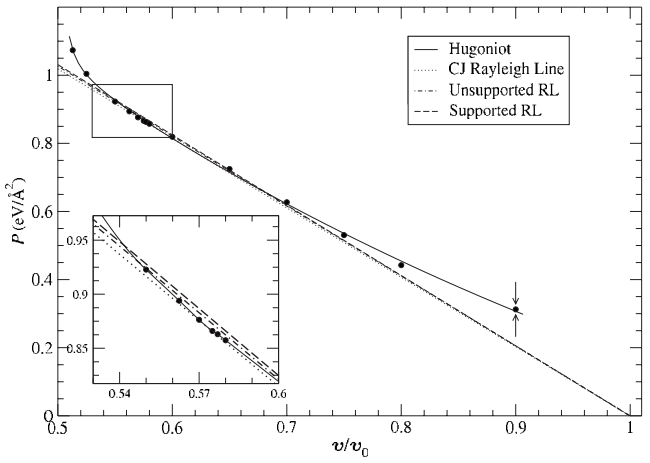

FIG. 3. A P-v state diagram of the equilibrium product Hugoniot. The solid curve is a guide to the eye. The dotted and dashed curves are Rayleigh lines plotted using the initial state (P_0=0.0, v/v_0=1.0) and a slope of $-u_s^2\rho_0$, where ρ is the mass density and u_s for each curve, from the steepest down, is the median value of shock velocity taken from the supported detonation, the unsupported detonation, and the EOS calculation. The arrows represent a series of simulations at constant v used to find the datum to which they point. The box is a magnification.

enough to include more than three data points in order to get a proper estimate of the error from the goodness-of-fit parameter.

To test the CJ results found from these *NVE* simulations, we run a supported detonation simulation in which an infinitely massive driving piston impacts the AB sample at the

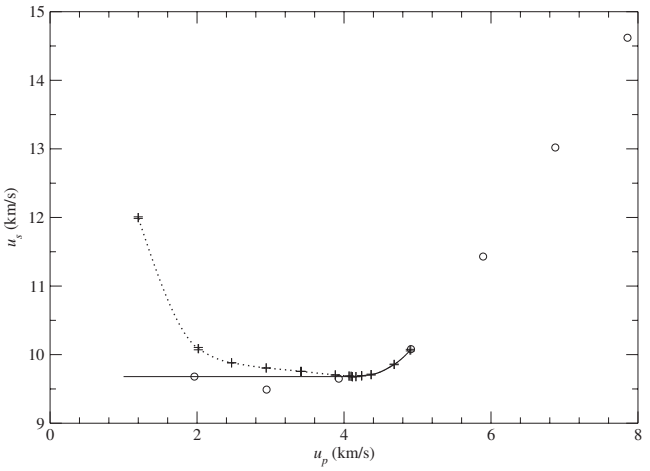

FIG. 4. Shock velocity (u_s) vs particle velocity (u_p). Similar plots can be made for other thermodynamic variables on the abscissa. Each point corresponds to a different value of specific volume (v), which increases along the abscissa in the direction opposite that of u_p. A constant line is drawn at the determined minimum value of u_s. The dotted part of the curve indicates that which is not dynamically accessible. Instead NEMD simulations with pistons moving at u_p less than the value at which the minimum is located ideally should follow the constant line. The open circles show the results of piston driven NEMD simulations where the piston is driven at u_p.

CJ-determined particle velocity (u_{pj}). This should establish a constant zone behind the front that should be at the CJ state, with the front propagating at the CJ conditions. Measurements are taken from this run and can be found in Table I under the "Supported NEMD" column. From Table I one can see that many of the values fall within error of one another, although there are some slight discrepancies. It should be noted that the supported NEMD simulations can include transients from the initiation and/or buildup processes [2], and these will be explored further below. Still, this discrepancy of 0.35% from the unsupported detonation of u_s =9.70961±0.00054 km/s is quite small. Previous evaluations of this same system gave estimated values of u_s as 9.3 km/s in [16] and 9.5 km/s in [17], with caveats that the systems may not yet have reached a steady-state condition. Having run longer, our simulations have come closer to a steady state, and this could account for our better agreement on this particular system. Ours is also less of an error than Rice *et al.* found for their variation of the REBO model. It is possible that their system may not have yet reached steady state in the NEMD simulations or that the reaction completion criterion is not met; they attribute their difference to asymmetry in the particle masses, a feature not present in the current parameterization.

We repeated several of the tasks performed on Q =3.0 eV for other values of Q. In Fig. 5 the equilibrium P-v Hugoniot for several values of Q are shown. Notice for Q =6.0 eV that the curve has a roughly hyperbolic shape, similar to what is observed for product gases of conventional HEs [2,13]. The CJ state for this value of Q is easy to determine. From it, as was done above, we find u_{sj} to be 12.20552±0.0020 km/s. The unsupported NEMD simulation with the free boundary gives 12.2031±0.0017 km/s, a difference that is smaller than the error bars. As Q decreases, the equilibrium Hugoniots flatten out, and it becomes more difficult to identify the exact point of tangency. At Q =2.0 eV the Hugoniot is well represented by a linear fit. The Hugoniot for Q=1.5 eV has a negative curvature (convex) section (Fig. 5), suggesting a phase transition. White *et al.* [20,30] have characterized what they describe as a dissociative phase transition in other variations of this REBO potential, and this phenomenon may be similar to that. It should be noted that Q=1.5 eV is close to Q_c, the value for which a detonation cannot be sustained.

A comparison of the predicted and measured values of u_s for different values of Q is given in Table II. It is found that there is good agreement between these values, with no discernible discrepancy for Q=6.0 eV and only a moderate discrepancy of 2% for Q=1.5 eV, which is near the failure point for the given initiation impact parameters. The latter point supports the idea that failure is occurring because of inadequate completion of the reaction when the sonic point passes. This decrease in the extent of the reaction will be strongly exacerbated by the decreased driving force (energy) of the reaction and the associated decreased shock temperature, which will dramatically slow the rate of reaction. This emphasizes a central assumption of the ZND model: that there be a finite-width reaction zone. Thus, modest discrepancies between observed and predicted behavior (as perhaps observed in Ref. [18]) are not indicative of a particularly

TABLE I. Values measured or defined in the process that determines the CJ state through a series of microcanonical equilibrium simulations or in the constant zone of a nonequilibrium simulation of a critically supported detonation (Sec. IV). v is the specific volume, u_s is the shock velocity, u_p is the particle velocity at the final state, T is the absolute temperature, U is the potential energy, E is the specific internal energy, and P is the 2D pressure. Values marked with asterisks are input into the corresponding simulation(s). The parentheses indicate the error in the last two digits of the corresponding reported value.

	CJ interpolation			Supported NEMD
Q (eV)	1.5*	3.0*	6.0*	3.0*
v/v_0	0.50182(24)	0.57164(81)	0.6171(19)	0.5747(16)
u_s (km/s)	8.0720(11)	9.6758(90)	12.2055(20)	9.7360(40)
u_p (km/s)	4.0212(13)	4.1446(40)	4.673(22)	4.144*
$\langle k_B T \rangle$ (eV)	0.4017(14)	0.7839(43)	1.7550(90)	0.7791(56)
$\langle U \rangle$ (eV)	−0.25156(79)	−0.5605(21)	−1.19657(90)	−0.5746(72)
$\langle E \rangle$ (eV)	0.15012(65)	0.2234(22)	0.5584(84)	0.2234306(15)
P (eV/Å^2)	0.70591(33)	0.8726(13)	1.2411(62)	0.8541(83)

inadequate or inappropriate model, but rather are likely showing that the ZND assumptions are not being rigorously fulfilled. We emphasize that the CJ assumption often provides good estimates for the detonation properties of high-performance explosives, but their absolute accuracy is not well known because of limitations in measurements and modeling [2,11–14]. Given the low level of discrepancy, one can conclude that these systems are responding in accordance with the simple predictions of the Chapman-Jouguet hypothesis. This is consistent with the expectations of White and co-workers for this model and their results on related systems [20].

What is of greatest significance here is that this shows that the variations in u_s with the molecular parameters are therefore determined by the CJ conditions. These are defined by the EOS of the products, as the initial state is not being modified. These aspects will now be examined in further detail. The curves in Figs. 3–5 are somewhat unusual. For an energetic material with typical product-gas behavior, the product Hugoniot would have a hyperbolic shape in P-v space (Figs. 3 and 5) and a parabolic shape in u_s—u_p space (Fig. 4). These are the types of curves observed for the current models of typical product materials [11–14]. Here, for large Q (=6 eV) the resulting curves do have that type of behavior. However, as Q is reduced, the Hugoniot flattens until it eventually gains a convex section, and the u_s-u_p plot evolves into a curve with a double minimum. Therefore, we examine the CJ states more closely by simulating a microcanonical ensemble at the determined CJ values of density and internal energy. We pursue this analysis for three reasons. First is that we wish to modify the current REBO potential so that it more accurately captures behavior typical of the conventional models for common explosives [2,11–14], which assume a molecular CJ state. Second is that we wish to understand the origins of the different shock structures that have been observed with this class of models. The last is that it is possible that these structures may represent some classes of explosives.

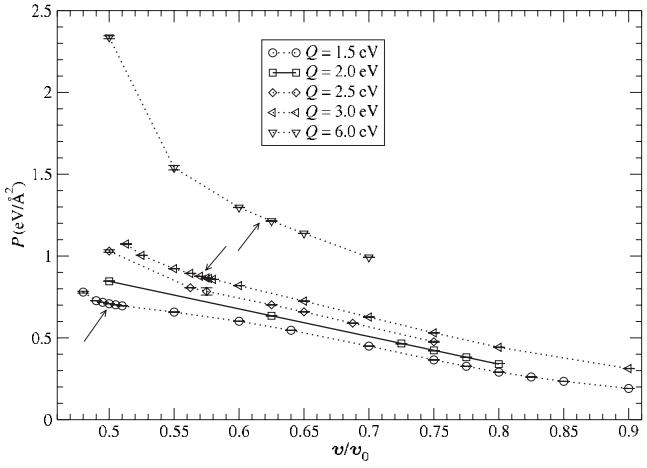

FIG. 5. Equilibrium Hugoniots for several values of Q. The CJ state is determined for the cases in which Q=6.0, 3.0, and 1.5 eV. The curve for Q=2.0 eV is well fit by a straight line of the form $P=1.69(1-v/v_0)$. The dotted lines are all guides to the eye. As Q decreases, the Hugoniots go from positive curvature to a zero curvature for Q=2.0. The curve for Q=1.5 eV contains a section of negative curvature, indicating a phase transition. The arrows point to the determined CJ states.

A snapshot of the NVE-at-CJ simulation for Q=3.0 eV is shown in Fig. 6, along with the corresponding radial distribution functions [RDFs, $g(r)$] for particles of the same and different type. It is evident from Fig. 6 that, at the CJ state, the system is dominated by short AA and BB contacts, which would be expected for the product species. The interatomic distances for these ($\approx 1.1 r_e$) are slightly larger than those

TABLE II. Comparison of shock velocities calculated for the CJ state (u_{sj}) determined by equilibrium simulations, summarized in Table I and observed in the NEMD simulations (u_s).

Q (eV)	u_{sj} (km/s)	u_s unsupported	% difference	Duration (ps)
1.5	8.0720(11)	7.913(16)	≈2.0	60
3.0	9.6758(90)	9.70961(54)	≈0.35	105
6.0	12.2055(20)	12.2032(17)	≈0.0	35

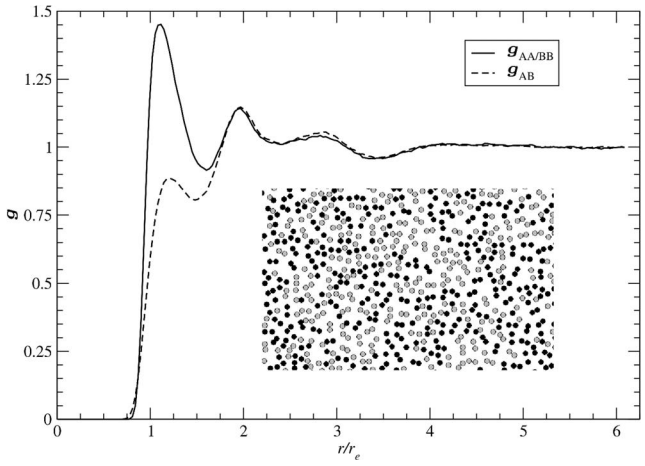

FIG. 6. Radial distribution function for the CJ state for $Q=3.0$ eV. g_{AB} measures the chance of finding particles of opposite types a distance r apart divided by the probability if the atoms were randomly distributed. $g_{AA/BB}$ indicates the probability of finding particles of the same type a distance r apart, again, divided by the probability if the distribution were random. The inset shows a section of a snapshot of the simulation. A atoms are black and B are gray.

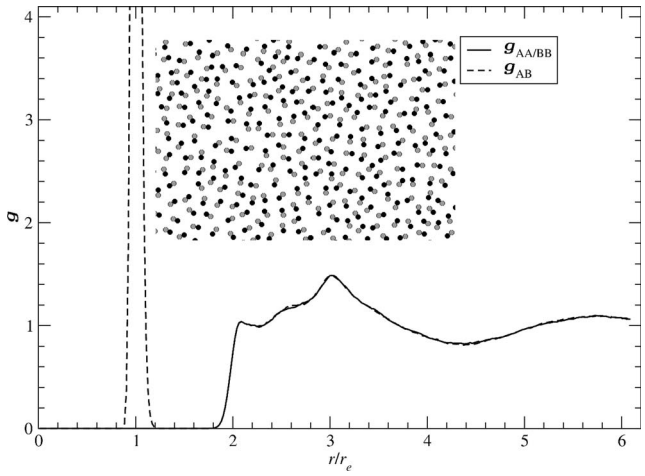

FIG. 7. RDF for melted AB. The first peak, the maximum of which is about 14, indicates the presence of dimers. The peak above $r/r_e=2$ is due to the inner cutoff spline in the V_{vdW} term of Eq. (1). The peak at $r/r_e=3$ is probably caused by the arrangement of dimers.

defined for the isolated molecules ($1.0r_e$). By the form of the potential, the introduction of a third particle within the defined bonding distance weakens the attractive part of the potential and moves the minimum of the bonding potential out to greater distances. What is more intriguing is that there is also a significant number of close A-B interactions at $\approx 1.2r_e$, showing that the system has not evolved into a simple mixture of A_2 and B_2. Also, there is a second peak in both RDFs at around $r/r_e=2.0$ as well as an additional one around $r/r_e=3.0$. This indicates that there are clusters of atoms forming at this compression. This suggests that there could be remnants of the dissociative state studied by White *et al.* using the initial version of the AB model [30] that are no longer able to lead to a rarefaction shock and concomitant flat-topped split-shock waves. The higher density dissocative state is not an atomization in the sense of isolated atoms but rather a state where the diatomic molecules tend to lose their diatomic molecular identity because of simultaneous but weaker interactions with a greater number of neighbors. In this state the number of close contacts increases but the nearest-neighbor distance also increases slightly because of weaker, more metalliclike bonding. As such, it is reminiscent of the metallization of H_2 at high pressures or perhaps a polymerization of CO_2. In any event, regardless of its precise interpretation, this clustering aspect probably accounts for the relatively high density at the CJ conditions here ($v/v_0 \approx 0.6$) compared to values for conventional organic high explosives ($v/v_0 \approx 0.75$), which are presumed to have molecular CJ states [2,11–14]. Other classes of materials might correspond to such clustered or dissociative states,[1] and it is important to understand the implications of such mechanisms.

[1]For example, it is proposed that lead azide detonations involve atomic species and dissociated electrons [36].

For comparison, Fig. 7 shows the RDF of a *NVE* simulation of AB at a temperature above its melting point and at the initial density $v=v_0$. It has a strong peak for the AB dimers at $r/r_e=1$ as expected. Beyond this, it was expected that there would be a broad peak at $2.8r_e$, which would be the van der Waals minimum. Although this was observed, somewhat surprisingly, there is a sharp peak just above $r/r_e=2$ which is present for all three atomic combinations, as well as another peak at $3r_e$. The former peak is probably caused by the positive slope of a section of the inner cutoff spline for the V_{vdW} term, which creates an additional minimum in the multibody potential. These attributes highlight some of the features that can arise from these complex interaction potentials and illustrate the difficulties in controlling detailed aspects of their behavior.

The notable difference between the RDFs is that the one for the melted AB goes to zero between $r/r_e=1.2$ and 1.8, which highlights the clear diatomic nature of that system. For the CJ state simulation, there is substantial intensity all across that region, and the RDF value barely drops below 1. Since there are no dissociated diatomic molecules or clusters in the melted AB, it is reasonable that we see a domain above $r/r_e=1$ in which a particle will not have a neighbor. Any third particle and its bound partner will be repelled by virtue of the V_A term if they approach much closer than $2r_e$ to a particle in another dimer. At the CJ state density, this repulsion breaks down and clusters of particles form. Similar behavior has also been observed in the systems that Rice *et al.* studied [18,19] and in the snapshots reported by Brenner *et al.* [16].

To examine this behavior more closely, we examine the RDFs along the Hugoniot. In particular, we consider the case of $Q=1.5$ eV, which has a convex section indicative of a phase transition. This convex section is similar to that observed by Swanson *et al.* in a related REBO model [32]. The RDFs for several states along that Hugoniot including $v/v_0=0.64$, the volume at which the phase transition occurs, are

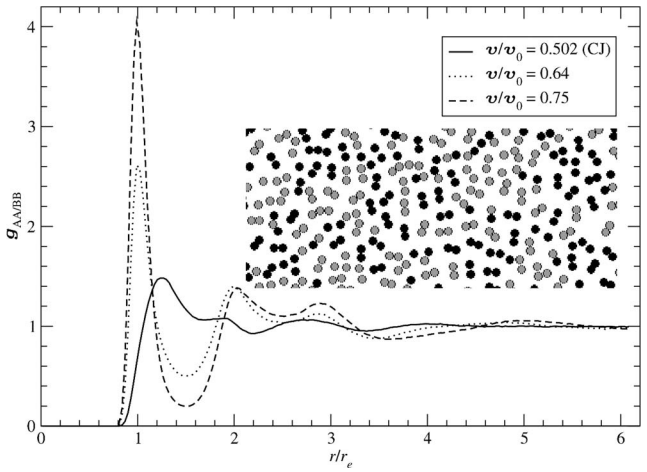

FIG. 8. Same-type radial distribution function for an exothermicity $Q=1.5$ eV at states along the Hugoniot at volumes shown. Notice the maximum at radial distance $r/r_e \approx 2.75$ for the CJ state. It represents the van der Waals equilibrium distance. The local minimum of the other curves at that point are still greater than unity. Notice the local maxima for the other two curves at $r/r_e=3.0$. They suggest tetramer formation or perhaps dimer alignment. The inset is a snapshot of the simulation for $v/v_0=0.64$.

shown in Fig. 8. For the CJ state, $v/v_0=0.502$, the RDF is similar to that for the CJ state at $Q=3.0$ eV. The first peak occurs at $1.2r_e$ with no strong minima occurring at longer distances. At $v/v_0=0.64$, a deep minimum develops at $\approx 1.5r_e$ along with peaks at $r/r_e=2.0$ and 3.0. From the snapshot at $v/v_0=0.64$ (see inset), both distinct dimers and clusters appear to be present. At $v/v_0=0.75$, the peak sharpening and minimum development are more distinct, and the profile is more reminiscent of the AB melt illustrated in Fig. 7.

As previously noted [16,18,19], there is a low activation barrier for the attack of the monomer A species on the A end of the AB molecule. This is entirely consistent with the expectations for the attack of an atomic or radical species on a molecular species and could be the major path of chemical reaction in this detonation. Assuming that this is the case, our interest here is how that path might be altered by changing the molecular properties. Changing the exothermicity of the reaction (Q) affects the activation barrier as one would expect (e.g., the Hammond postulate): increasing the exothermicity decreases the activation energy (E_a) and increases the likelihood of reaction. This and the dependence of E_a on the dissociation energy (D_e^{AB}) are given in Table III. There it is shown that E_a increases with increasing D_e^{AB}, thus depressing the likelihood of a reaction. This would rationalize that, as D_e^{AB} is increased, the material eventually fails to detonate, given the same initiator strength.

IV. EXOTHERMICITY'S RELATION TO EOS

We now turn to understanding the linear relation between u_s^2 and Q. One simple model is suggested by Fickett and Davis [1], who derive a linear relation between Q and u_s^2 by adding Q to the incomplete equation of state of the initial state of a polytropic gas, an ideal gas with a constant specific heat. An expression for the change in specific internal energy becomes $E-E_0=(Pv-P_0v_0)/(\gamma-1)-Q$, where γ is the adiabatic gamma [37]. One can then eliminate $E-E_0$ with the Hugoniot jump condition [Eq. (4)], thus solving for P. It is assumed that $P_0=0$. One can use the condition that the Rayleigh line be tangent to the Hugoniot at the CJ state to arrive at $u_s^2=2(\gamma^2-1)Q/m$, where m is the mass of the reactants. If it is assumed that this EOS accurately describes our potential, $\gamma \approx 2$. A typical conventional HE has a $\gamma \approx 3$ [2]. Since the volume at the CJ state is given by the expression $v/v_0=\gamma/(\gamma+1)$, this relationship does rationalize the somewhat greater compression observed here ($v/v_0<0.67$) compared to that for conventional HEs ($v/v_0 \approx 0.75$). (It should be noted that the values of v/v_0 given in Table I are smaller yet and imply a value of $\gamma \approx 1$.) However, since we have demonstrated that the product's Hugoniot does not behave like that of an ideal gas, this argument does not provide a sound basis to explain the observed between u_s^2 and Q.

TABLE III. The minimum peak value of the barrier to be overcome for the collinear reaction $\mathrm{AB+B \rightarrow A+B_2}$ (or equivalently $\mathrm{A+AB \rightarrow A_2+B}$) ($E_{a,0}$, where the second subscript indicates the supplementary angle between AB and BB) for several values of D_e^{AB} and Q. For the first two columns $Q=3.0$ eV. For the second two columns $D_e^{\mathrm{AB}}=2.0$ eV. Detonation cannot be initiated at $D_e^{\mathrm{AB}}=4.0$ eV for the given flyer thickness and velocity. All of the measurements of $E_{a,0}$ have an error of ±0.0025 eV.

D_e^{AB} (eV)	$E_{a,0}$	Q (eV)	$E_{a,0}$
0.5	0.0125	1.5	0.1675
1.0	0.0125	2.0	0.1275
1.5	0.0225	2.5	0.0975
2.0	0.0775	3.0	0.0775
2.5	0.1625	3.5	0.0575
3.0	0.2725	4.0	0.0425
3.5	0.4025	6.0	0.0125
4.0	0.5475	10.0	0.0125

An alternative explanation is suggested by an examination of the Hugoniot curves shown in Fig. 5. There, in the region of $0.55<v/v_0<0.7$ (which spans the region containing the CJ states), there appears to be an approximately linear offset of the curves. This suggests that a Mie-Grüneisen EOS form with an unspecified reference Hugoniot might be suitable, where it is assumed that the value of Γ/v is dependent on v. Truncating the Taylor expansion around a reference Hugoniot as in [37], we get

$$P \approx P_R + \Gamma(E-E_R)/v, \tag{7}$$

where the Grüneisen gamma

$$\Gamma \equiv v\left(\frac{\partial P}{\partial E}\right)_v. \tag{8}$$

We substitute Eq. (4) into Eq. (7) and, because we take E as relative to the products, set $E_0=q$, where q is the specific heat of reaction. Upon rearrangement we get for the P-v Hugoniot

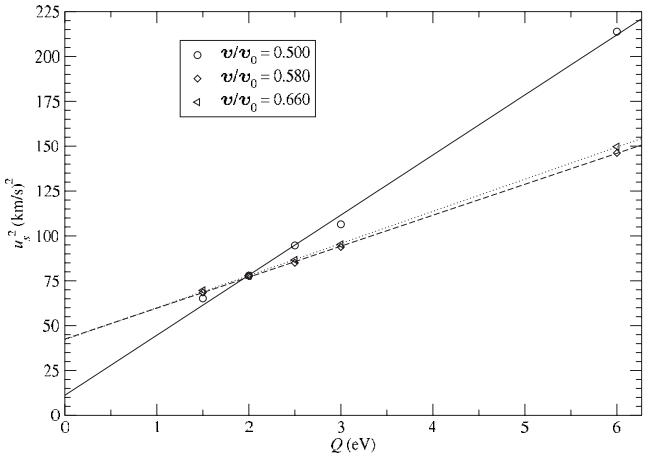

FIG. 9. Square of the shock velocity (u_s^2) vs exothermicity (Q) for select constant values of specific volume (v). The lines are linear fits. Notice that the fit is better for the higher values of v. Notice, also, that the lines cross at $v/v_0=2.0$ eV. This indicates a linear dependence between the slopes and the y intercepts.

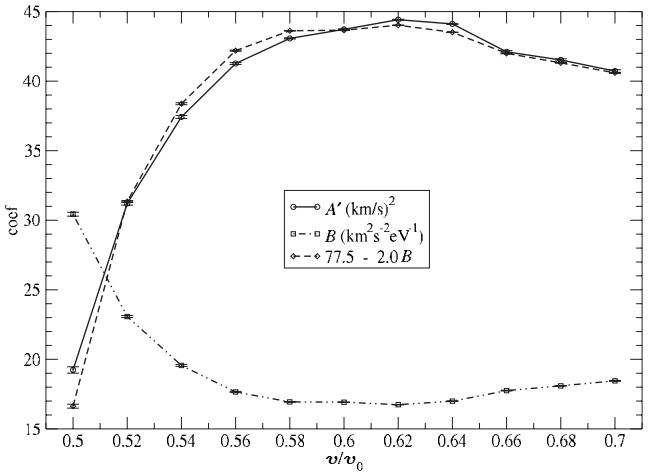

FIG. 10. Coefficients of the fits as described in Fig. 9 vs specific volume for $D_e^{\mathrm{AB}}=2.0$ eV. A' is the y intercept and, as in Eq. (11), B is the slope. The dashed line is the calculation shown in the legend.

$$P_H = \frac{1}{v\left(1-\frac{\Gamma}{2}\frac{v_0-v}{v}\right)}[vP_R+\Gamma(q-E_R)]. \tag{9}$$

Utilizing Eqs. (5) and (6), we can derive

$$u_s^2 = P_H\frac{v_0}{1-\frac{v}{v_0}}. \tag{10}$$

This yields, for this class of EOS, the general expression

$$u_s^2 = A(v,\Gamma)P_R + B(v,\Gamma)(q-E_R). \tag{11}$$

It should be noted that q does not necessarily equal Q/m. In the case where the bond order parameter $B_{ij}=1.0$ for the initial state, Q/m should be q less the small contribution of the van der Waals interaction. When we run a *NVE* simulation of 1250 AB molecules at the initial state used in the NEMD simulations, we find a total internal energy of −2548.5 eV. Where Davis measures the zero of energy as cold products [37], our calculations use a zero of cold dissociated atoms. Our measurement here finds $E_0 \approx D_e^{\mathrm{AB}}$ and is consistent with $B_{ij}=1.0$ and a 2% van der Waals contribution of a few neighbors; therefore, $Q/m \approx q$ to good order, and the two can be used interchangeably.

The validity of this Mie-Grüneisen approximation can be tested by the linear dependence of u_s^2 on Q for constant volumes. A few of these plots are given in Fig. 9, which shows that good linear relationships are found for the three selected volumes. This shows that the Mie-Grüneisen EOS is a good approximation for our model for low v (high compressions). Since the data were generated during the process of seeking the minimum u_s for each Q, interpolation was used to find values at common abscissas. The coefficients of the fits generated by the method in Fig. 9 are then plotted in Fig. 10 vs v/v_0. Here, A' is the y intercept of those linear fits and B is the slope. The value A' is distinct from A in Eq. (11) because it now includes a contribution from E_R. However, the value of B is exactly the same as defined in that equation. The fact that all of the lines in Fig. 9 cross at $Q=2.0$ eV leads one to conclude that A' and B are linearly dependent. The third curve in Fig. 10 is an attempt to show this for the relation $A'=77.5-2.0B$.

The net result of this analysis is that, over the range of $0.55<v/v_0<0.7$, B is reasonably constant with a value of 17–19 (km/s)^2/eV. This result, inserted back into Eq. (11), is then in good agreement with the initial observation shown in Fig. 2, that the slope of the dependence of u_s^2 on Q is ≈19 (km/s)^2/eV. The ability to approximate the product EOS as linear Mie-Grüneisen offsets of one another, at least in the region near the CJ states, clarifies the origin of this linear dependence for this system and establishes a quantitative explanation for the observed slope.

Using Eqs. (9)–(11), we can then solve for Γ to find

$$\Gamma(v) = \frac{2B\left(1-\frac{v}{v_0}\right)\frac{v}{v_0}}{2+B\left(1-\frac{v}{v_0}\right)^2} \tag{12}$$

and plot the result in Fig. 11. Solving for B we have

$$B(v) = \frac{\Gamma}{\left(1-\frac{v}{v_0}\right)\left[1-\frac{\Gamma}{2}\left(1-\frac{v}{v_0}\right)\right]}. \tag{13}$$

Note that $(1-v/v_0)$ is the compression. From these equations, it can be seen that a constant value of B does not specify a constant value of Γ, but rather a particular dependence of Γ on v. Conversely, a constant value of Γ would also specify a particular dependence of B on v. However, from these two figures it is observed that both B and Γ are rather weak functions of v in the CJ region. This aspect of the EOS behavior (which we are unable to directly control) is important in the origin of the linear dependences observed in Fig. 2.

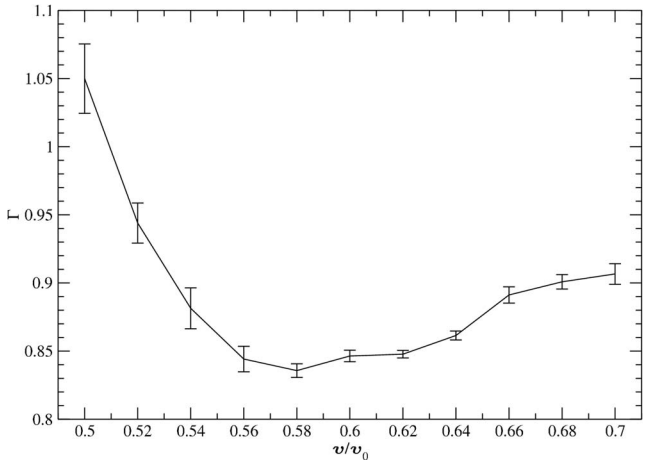

FIG. 11. Grüneisen Γ vs specific volume for $D_e^{AB}=2.0$ eV.

V. REACTION ZONE THICKNESS AND RATE STICK FAILURE DIAMETER

Having established the steady-state properties of these systems, we now turn to the transient properties related to the reaction zone thickness. There are two means that could be employed to determine the character of the reaction zone for these simulations. The most direct means is to drive the system with a piston whose velocity is matched to that of the CJ conditions. In this case, the one-dimensional profile should exhibit a rapid shock rise up to the vNS, followed by a relaxation to the CJ state, which is then a constant zone that extends back to the piston. There will be some transients present because the initiation process incurs a slight delay so that an equilibrium state is not immediately established, but otherwise this is a direct method if the CJ conditions are known. It is less direct to study a system with either an underdriven piston or perhaps initiated with a flyer plate. Such systems will initially propagate at less than the CJ conditions because the release waves erode the tail of the reaction zone. As the detonation proceeds and the release Taylor wave becomes more spread out (approximating a more steady condition behind the reaction zone), these will eventually "build up" to a steady detonation. It can be difficult to determine exactly when the system has evolved to a steady-state condition.

A comparison of these two approaches is shown in Fig. 12. For the case of a piston matched to the CJ conditions, a steady solution evolved quite rapidly as determined by both the detonation velocity and the constant properties of the following zone. The reaction zone, defined to be the distance from the shock front to the point where the transient properties are not distinguishable from the thermal fluctuations of the constant zone, extends out to ≈300 Å. A somewhat better characterization is probably the distance at which the particle velocity has decreased to $1/e$ of the initial overshoot. This occurs at ≈60 Å behind the shock front, or a characteristic time constant of 0.7 ps. For the transient simulations, it is apparent that the system is continuing to evolve even after propagating for 100 ps. The reaction zone length (emphasized in the inset) is clearly extending past 100 Å. (The

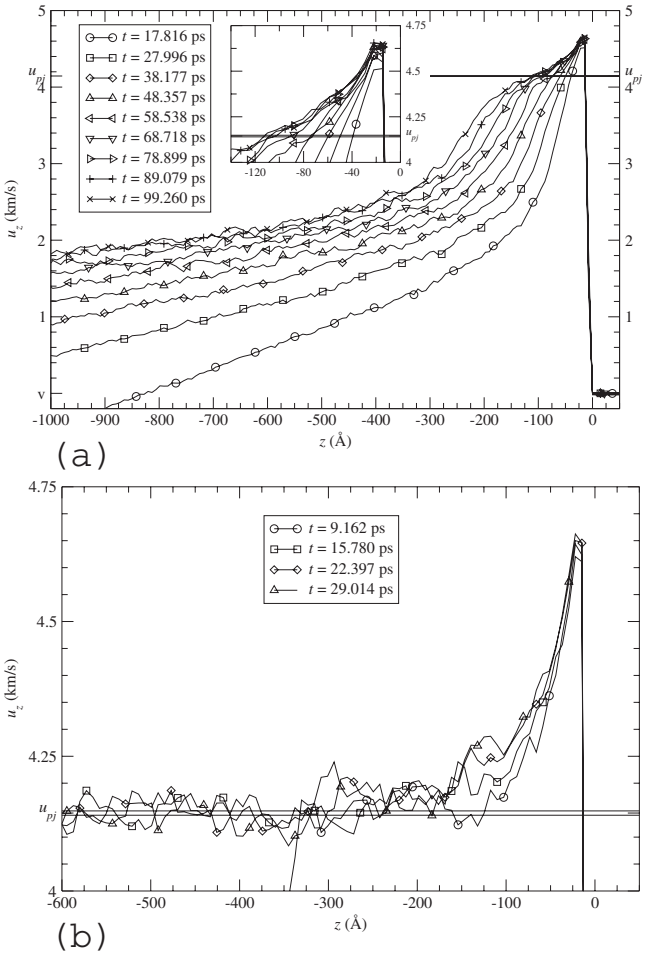

FIG. 12. (a) 129 profiles of the particle velocity in the z direction (u_z) separated in time by 50.9 fs are overlapped onto their center profile (whose time is indicated in the legend) such that their fronts line up. They are averaged, and nine of those averages are similarly overlapped. The simulation represented has the default parameterization for the REBO potential [16]. It is a flyer-driven unsupported simulation as described in Sec. II. Found for this specific parameterization in Sec. IV, u_{pj} is indicated by a constant line segment. The inset is a magnification of the region containing the von Neumann spike and the CJ state. (b) Similar profiles for a critically supported detonation. This simulation is shorter and thinner than in (a), but it suggests that (a) is not yet steady, since the profiles do not seem to settle down to u_{pj} until about 300 Å behind the front.

structure in the particle velocity plot after the reaction zone is likely due to the clustered chemical structure of the CJ state and could be characterized as a pseudophase transition back to the resolved diatomic A_2 and B_2 products.) As noted above, our measurements of the detonation velocity provide values slightly larger than those measured by White *et al.* [20] for the same model. They include in their calculations a time domain in which the detonation is still subtly building, as we show here, and they recognized this possible limitation in their evaluations. We, in fact, measure a detonation velocity (9.5580±0.0013 km/s) close to theirs (9.5 km/s) for the unsupported case if we include the front positions at 10 ps

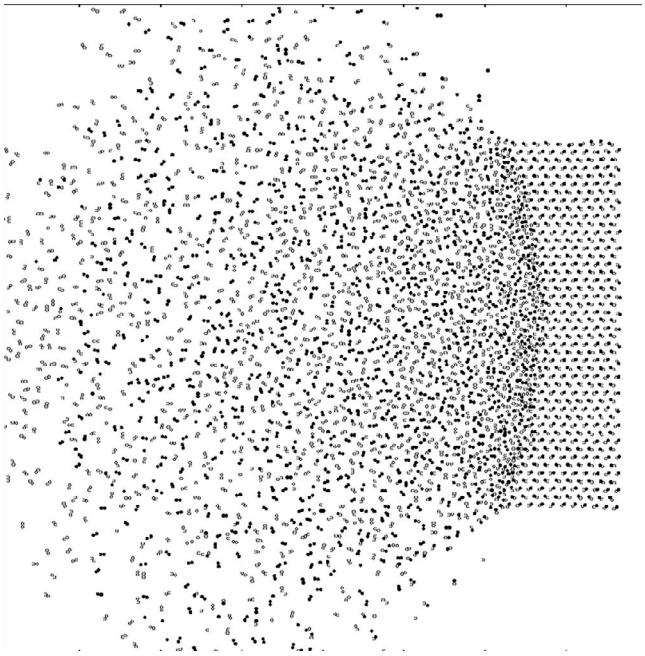

FIG. 13. Two-dimensional rate stick at supercritical width for $Q=3.0$ eV.

$<t<20$ ps in the linear least-squares fitting that determines u_s. This highlights the difficulties in using this approach of unsupported detonations to quantitatively determine the CJ properties, though the consequent dynamic aspects are highly relevant to real systems and measurements.

It should be noted that the transient system exhibits the classic buildup behavior quite nicely. In addition to the extension of the reaction zone out to its equilibrium value, there is also the gradual increase in the initial shock state up to its equilibrium value. As this sets the initial temperature and rate for the reaction chemistry, it emphasizes the significance of these transient phenomena. The shock velocity is also a sensitive indicator of the buildup process. While the deprecation of the velocity below the steady-state value is not great nor readily obvious, it can be discerned by careful observation. Previously reported discrepancies between the expected and observed CJ performances may well have been due to those systems not having fully attained steady-state conditions [18], though other factors could also be contributing.

Davis [38] showed that surface effects adversely affect a detonation's ability to propagate because rarefaction waves from the side release erode the reaction zone and its support structure. For cylindrical charges, this is characterized as a failure diameter below which detonation cannot propagate. White *et al.* demonstrated that when the periodic boundaries are removed from the sample so that the particles are free to escape the system, there exists a critical width (W_c) that the sample must exceed in the direction perpendicular to the propagation of the shock front (in our case $\hat{x}$) in order that the detonation be sustained. If the sample is too thin, rarefaction waves quench the detonation [17]. Figure 13 shows an example of a 2D rate stick at supercritical width while Fig. 14 displays a time series of the failure of a subcritical rate stick.

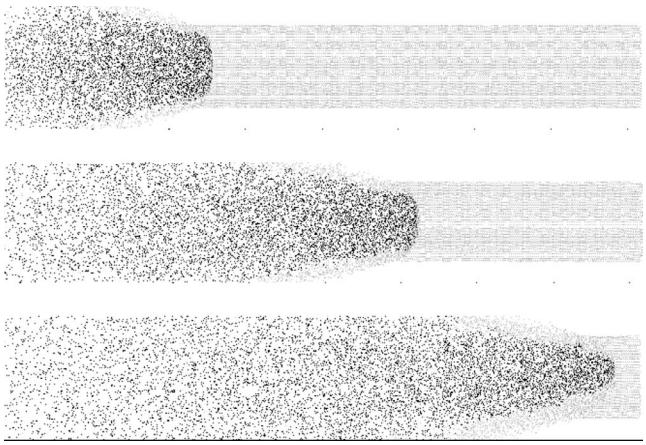

FIG. 14. Three sequential snapshots of a 2D rate stick at subcritical width. Here the particles are colored by bond type. Gray is unreacted, and black is reacted. Rarefaction waves from the rate stick's edge erode the reaction zone thus quenching the detonation.

The dependence of W_c on Q [25] and D_e^{AB} is shown in Fig. 15. Contrary to previous work [25], a curve of the form $y=a/(x-Q_c)$, rather than an exponential form, is fit to the data for Q. Other forms provide better fits, but this form is inspired by Hubbard and Johnson's [39] dependence of the delay time (t_d) (described below) on Q. This form is also asymptotic at the point where detonation is known to fail for an infinitely thick sample (Q_c). For D_e^{AB} a curve of the form $y=a(e^{bx}-1)/(x-D_{ec}^{\mathrm{AB}})$ is fit to the data for similar reasons. If Q is raised, the reaction should be more difficult to quench because there is more energy available to break neighboring AB bonds, and the activation energy for reaction is likely depressed. The reaction is expected to be faster and the reaction zone shorter because of the higher temperature resulting from the greater energy release. As Q lowers toward Q_c,

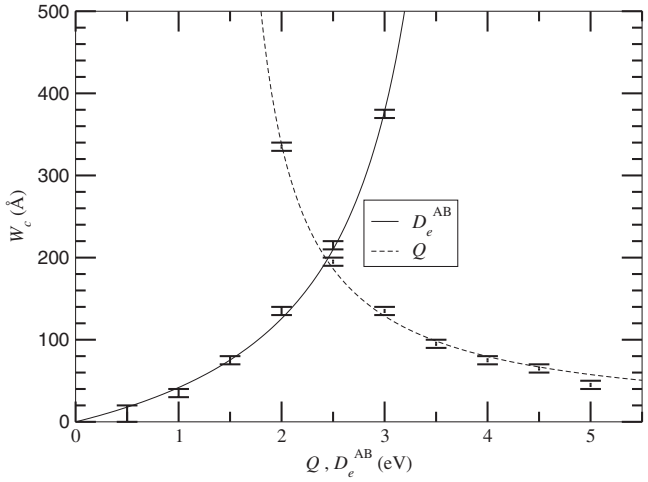

FIG. 15. Critical width (W_c) vs AB dissociation energy (D_e^{AB}) and exothermicity (Q). The upper dash of the error bar indicates the thinnest sample to sustain detonation. The lower error bar indicates the thickest sample to fail within 360 lattice spaces. The resolution is 10 Å. The lines are guides to the eye with empirical functional forms discussed in the text.

no matter how wide the sample is, detonation will not be sustained. On the other hand, if D_e^{AB} is lowered, it is harder for rarefaction waves to quench the detonation front because atoms dissociate more readily and the subsequent reactions should become more facile. W_c is thus lowered because detonation is more easily sustained. As it rises, D_e^{AB} reaches a critical value (D_{ec}^{AB}) (probably dependent on Q, flyer thickness and velocity, etc.) above which detonation cannot be sustained, no matter how wide the sample.

Using the idea of delay time (t_d), during which a reactant must remain above a certain temperature in order for a reaction to occur, Hubbard and Johnson [39] give an example of how a detonation's ability to be initiated or sustained may depend on Q and D_e^{AB}. We use this in lieu of finding reaction rate data. The longer this time, the less likely the reaction. In their example, t_d has an inverse dependence on Q and an inverse and exponential dependence on activation energy E_a:

$$t_d = \frac{RE_0^2}{c_v \nu E_a Q} \exp\left(\frac{c_v E_a}{RE_0}\right), \tag{14}$$

where ν is the collision rate, R is the molar gas constant, c_v is the specific heat at constant volume, and E_0 is the internal energy behind the shock [39].

In Rosing-Chariton theory, when $\Theta = t_r$, $d = W_c$, where $\Theta = d/2c$ is the scattering time, t_r is the reaction time, c is the speed of sound, and d is the diameter of the sample. The rate stick must be thick enough that rarefaction waves, traveling at c from the surface, cannot sufficiently penetrate the HE in order to scatter the reaction zone and quench the reaction in a time equal to the reaction time. The width of the chemical reaction zone $a = t_r(u_s - \bar{u})$, where $\bar{u}$ is the average particle velocity in $\hat{z}$ within the zone and u_s is the velocity of the detonation front. Replacing t_r with Θ, one finds

$$W_c = d = 2ca/(u_s - \bar{u}), \tag{15}$$

where u_s is a function of d [20,38,40]. If $t_d \propto t_r$ and $E_a \propto D_e^{\mathrm{AB}}$, we find that $W_c \propto t_d$, supporting our selection of curve fits.

To check the validity of Eq. (15), we use for a the characteristic decay length of the reaction zone (60 Å) determined above. If the ratio $2c/(u_s - \bar{u}) \sim 2$, this would be excellent agreement. As the value of $u_s - \bar{u}$ should be approximately equal to the local sound speed, this estimation is then quite good. Given the approximations involved in making this assessment, this is a fortuitous level of agreement, but can be taken as support for this analysis. Overall, a more thorough understanding of these phenomena is emerging through these studies.

VI. CONCLUSION

We have analyzed the relations between the energetic chemical properties of a simple, but well studied, class of high-explosive molecular models and the physical properties of the resulting detonation characteristics through explicit molecular dynamics simulations. This provides an excellent means to compare to the results of continuum analyses and avoids the complication of a multiphase equation of state and other approximations required in those approaches. Our approach was to vary two fundamental molecular quantities, the exothermicity and the reactant dissociation energy, and determine how those affected the macroscopic properties. Previous studies within this class [18,32] had shown that these types of systems behave consistently with the CJ and ZND detonation models and showed changes in behavior with molecular parameters. Our observations for the current class of models are the following.

(i) We observe simple and direct changes of detonation velocity with these molecular quantities.

(ii) These variations are consistent with the CJ and ZND models, which means that the changes must be attributable to how the product EOS is modified (given that the molecular properties of the starting materials have not been altered to any observable extent). We have demonstrated the changes in the CJ state of product EOS directly and quantified the physical origin of the variations.

(iii) The failure points (and the precedent falloff from the linear correlations) are consistent with molecular changes that lead to decreased chemical reaction rates and to as much as a 2% difference between shock velocities calculated for the CJ state determined by equilibrium simulations and those determined by NEMD simulations.

(iv) The reaction zone was determined to have a length $\approx$300 Å (or to have a charateristic decay length $\approx$60 Å) from steady-state calculations (i.e., supported with a piston moving at the CJ particle velocity), and it requires extended times to reach these lengths for unsupported detonations.

(v) The failure diameter was also found to have simple and direct dependences on these two molecular properties, Q and D_e^{AB}, its value justified in terms of the observed characteristic decay length of the reaction zone.

(vi) For this particular model we see no obvious sign of any 1D or 2D instabilities, which could be present in more complex detonation models [7–10].

In the process of this study, we have characterized some properties of the current molecular model which differ from expected behavior for conventional high explosives. These are, in particular, a CJ state consisting of nonmolecular species and product Hugoniot curves that behave significantly differently from simple nonideal gas behavior. The expectations here are based on models for conventional, organic high explosives that presume a molecular state for the CJ conditions and adequately predict those properties based on that assumption [2,11–14]. The predicted and experimentally validated product expansion curves for those systems show behavior consistent with those molecular models. Despite this, we have observed general consistency between the MD approach and the thermodynamic equations. Given that the fundamental CJ and ZND models pose minimal constraints on the behavior of chemical systems, this result reinforces the limited physical assumptions required for those derivations.

ACKNOWLEDGMENTS

The authors would like to thank Sam Shaw, Alejandro Strachan, Jerry Erpenbeck, Tommy Sewell, Shirish Chitanvis, Tamer Zaki, Yogesh Joglekar, Ben Haley, Rolando Somma, and David Hall for useful conversations. This material was prepared under Contract Nos. W-7405-ENG-36 and DE-AC52-06NA25396 with the U.S. Department of Energy. The authors particularly wish to recognize funding provided through the ASC Physics and Engineering Modeling program.

[1] W. Fickett and W. C. Davis, *Detonation* (University of California Press, Berkeley, 1979).
[2] C. L. Mader, *Numerical Modeling of Detonations* (University of California Press, Berkeley, 1979).
[3] W. C. Davis, Sci. Am. **256**, 106 (1987).
[4] Y. B. Zeldovich and A. S. Kompaneets, *Theory of Detonation* (Academic, New York, 1960).
[5] J. von Neumann, in *John von Neumann, Collected Works*, edited by A. J. Taub (Macmillan, New York, 1942), Vol. 6.
[6] W. Doering, Ann. Phys. **43**, 421 (1943).
[7] J. J. Erbenbeck, Phys. Fluids **13**, 2007 (1970).
[8] H. I. Lee and D. S. Stewart, J. Fluid Mech. **216**, 103 (1990).
[9] M. Short and D. S. Stewart, J. Fluid Mech. **368**, 229 (1998).
[10] M. B. Short, http://www.galcit.caltech.edu/~jeshep/icders/cd-rom/EXTABS/262_20TH.PDF
[11] L. E. Fried and P. C. Souers, Propellants, Explos., Pyrotech. **21**, 215 (1996).
[12] W. M. Howard, L. E. Fried, and P. C. Souers *Proceedings, Eleventh International Detonation Symposium 1998*, edited by J. M. Short and J. E. Kennedy, ONR 33300-5 (Office of Naval Research, Arlington, VA, 2000), pp. 998–1006.
[13] G. L. Schott, M. S. Shaw, and J. D. Johnson, J. Chem. Phys. **82**, 4264 (1985).
[14] F. H. Ree, J. Chem. Phys. **81**, 1251 (1984).
[15] M. L. Elert, D. M. Deaven, D. W. Brenner, and C. T. White, Phys. Rev. B **39**, 1453 (1989).
[16] D. W. Brenner, D. H. Robertson, M. L. Elert, and C. T. White, Phys. Rev. Lett. **70**, 2174 (1993); , Phys. Rev. Lett. **76**, 2202(E) (1996).
[17] C. T. White, D. H. Robertson, D. R. Swanson, and M. L. Elert, in *Shock Compression of Condensed Matter—1999*, edited by M. D. Furnish, L. C. Chhabildas, and R. S. Hixson, AIP Conf. Proc. No. 505 (AIP, Melville, NY, 2000), p. 377.
[18] B. M. Rice, W. Mattson, J. Grosh, and S. F. Trevino, Phys. Rev. E **53**, 611 (1996).
[19] B. M. Rice, W. Mattson, J. Grosh, and S. F. Trevino, Phys. Rev. E **53**, 623 (1996).
[20] C. T. White, D. R. Swanson, and D. H. Robertson, in *Chemical Dynamics in Extreme Environments*, edited by R. A. Dressler (World Scientific, Singapore, 2001), p. 547.
[21] P. Maffre and M. Peyrard, Phys. Rev. B **45**, 9551 (1992).
[22] J. J. Erpenbeck, Phys. Rev. A **46**, 6406 (1992).
[23] D. H. Robertson, D. W. Brenner, and C. T. White, Phys. Rev. Lett. **67**, 3132 (1991).
[24] P. J. Haskins and M. D. Cook, in *High-Pressure Science and Technology—1993*, edited by S. C. Schmidt, J. W. Shaner, G. A. Samara, and M. Riss, AIP Conf. Proc. No. 309 (AIP, New York, 1994), p. 1341.
[25] P. J. Haskins, M. D. Cook, J. Fellows, and A. Wood, *Proceedings, Eleventh International Detonation Symposium 1998*, edited by J. M. Short and J. E. Kennedy, ONR 33300-5 (Office of Naval Research, Arlington, VA, 2000), pp. 897–903.
[26] T. C. Germann, B. L. Holian, P. S. Lomdahl, A. J. Heim, N. Grønbech-Jensen, and J.-B. Maillet, *Proceedings, Twelfth International Detonation Symposium 2002*, edited by J. M. Short, ONR 333-05-2 (Office of Naval Research, Arlington, VA, 2005), pp. 711–717.
[27] B. L. Holian, T. C. Germann, J.-B. Maillet, and C. T. White, Phys. Rev. Lett. **89**, 285501 (2002); **90**, 069902(E) (2003).
[28] J.-B. Maillet, B. Crouzet, C. Matignon, L. Mondelain, and L. Soulard, in *Shock Compression of Condensed Matter—2003*, edited by M. D. Furnish, Y. M. Gupta, and J. W. Forbes, AIP Conf. Proc. No. 706 (AIP, Melville, 2004), pp. 385–388.
[29] C. T. White, J. J. C. Barrett, J. W. Mintmire, M. L. Elert, and D. H. Robertson, in *Shock Compression of Condensel Matter*, edited by S. C. Schmidt and W. C. Tao, AIP Conf. Proc. No. 370 (AIP, Woodbury, NY, 1996), pp. 187–190.
[30] C. T. White, D. H. Robertson, M. L. Elert, and D. W. Brenner, in *Microscopic Simulations of Complex Hydrodynamic Phenomena*, edited by M. Mareschal and B. L. Holian (Plenum, New York, 1992), p. 111.
[31] J. Tersoff, Phys. Rev. Lett. **56**, 632 (1986); Phys. Rev. B **37**, 6991 (1988).
[32] D. R. Swanson, M. L. Elert, and C. T. White, in *Shock Compression of Condensed Matter—1999* [17], p. 385.
[33] P. S. Lomdahl, P. Tamayo, N. Grønbech-Jensen, and D. M. Beazley, in *Proceedings of Supercomputing 93*, edited by G. S. Ansell, (IEEE Computer Society Press, Los Alamitos, CA, 1993), p. 520.
[34] M. L. Elert, D. H. Robertson, and C. T. White, in *Decomposition, Combustion, and Detonation Chemistry of Energetic Materials*, edited by T. B. Brill, T. P. Russell, W. C. Tao, and R. B. Wardle, MRS Symposia Proceedings No. 418 (Materials Research Society, Pittsburgh, 1996), p. 309.
[35] M. L. Elert, J. J. C. Barrett, D. H. Robertson, and C. T. White, in *Shock Compression of Condensed Matter—1997*, edited by S. C. Schmidt, D. P. Danleker, and J. W. Forbes, AIP Conf. Proc. No. 429 (AIP, Woodbury, NY, 1998), p. 293.
[36] D. Heflinger, I. Bar, T. Ben-Porat, G. Erez, and S. Rosenwaks, J. Appl. Phys. **73**, 2138 (1993).
[37] W. C. Davis, in *Explosive Effects and Applications*, edited by J. A. Zukas and W. P. Walters (Springer-Verlag, New York, 1998), p. 47.
[38] W. C. Davis, Los Alamos Sci. **2**, 48 (1981).
[39] H. W. Hubbard and M. H. Johnson, J. Appl. Phys. **30**, 765 (1959).
[40] A. N. Dremin, *Toward Detonation Theory* (Springer-Verlag, New York, 1999).